Direct Imaging of Charge Transport in Progressively Reduced Graphene Oxide Using Electrostatic Force Microscopy

Sibel Ebru Yalcin,[*,†,#] Charudatta Galande,[‡] Rajesh Kappera,[§] Hisato Yamaguchi,[⊥] Ulises Martinez,[⊥] Kirill A. Velizhanin,[∥] Stephen K. Doorn,[†] Andrew M. Dattelbaum,[⊥] Manish Chhowalla,[§] Pulickel M. Ajayan,[‡] Gautam Gupta,[⊥] and Aditya D. Mohite[*,⊥]

[†]Center for Integrated Nanotechnologies, Materials Physics and Applications Division, Los Alamos National Laboratory, Los Alamos, New Mexico 87545, United States, [‡]Department of Materials Science & NanoEngineering, Rice University, Houston, Texas 77005, United States, [§]Department of Material Science & Engineering, Rutgers University, Piscataway, New Jersey 08854, United States, [⊥]MPA-11 Materials Synthesis and Integrated Devices, Materials Physics and Applications Division, Los Alamos National Laboratory, Los Alamos, New Mexico 87545, United States, and [∥]T-1 Physics and Chemistry of Materials, Theoretical Division, Los Alamos National Laboratory, Los Alamos, New Mexico 87545, United States. [#]Present address: Pacific Northwest National Laboratory, Environmental and Molecular Science Laboratory, Richland, WA 99352, USA.

ABSTRACT Graphene oxide (GO) has emerged as a multifunctional material that can be synthesized in bulk quantities and can be solution processed to form large-area atomic layered photoactive, flexible thin films for optoelectronic devices. This is largely due to the potential ability to tune electrical and optical properties of GO using functional groups. For the successful application of GO, it is key to understand the evolution of its optoelectronic properties as the GO undergoes a phase transition from its insulating and optically active state to the electrically conducting state with progressive reduction. In this paper, we use a combination of electrostatic force microscopy (EFM) and optical spectroscopy to monitor the emergence of the optoelectronic properties of GO with progressive reduction. EFM measurements enable, for the first time, direct visualization of charge propagation along the conducting pathways that emerge on progressively reduced graphene oxide (rGO) and demonstrate that with the increasing degree of reduction, injected charges can rapidly migrate over a distance of several micrometers, irrespective of their polarities. Direct imaging reveals the presence of an insurmountable potential barrier between reduced GO (rGO) and GO, which plays the decisive role in the charge transport. We complement charge imaging with theoretical modeling using quantum chemistry calculations that further demonstrate that the role of barrier in regulating the charge transport. Furthermore, by correlating the EFM measurements with photoluminescence imaging and electrical conductivity studies, we identify a bifunctional state in GO, where the optical properties are preserved along with good electrical conductivity, providing design principles for the development of GO-based, low-cost, thin-film optoelectronic applications.

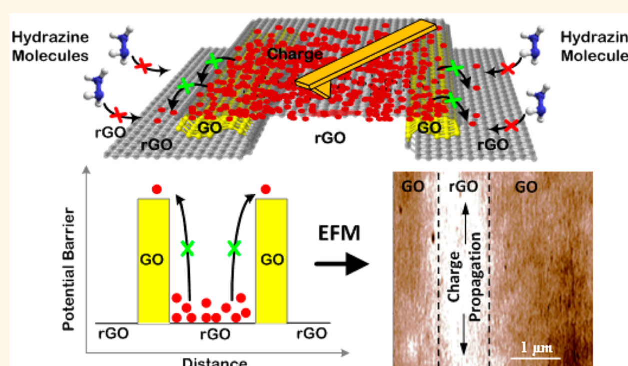

KEYWORDS: progressively reduced graphene oxide · charge injection · charge transport · electrostatic force microscopy (EFM) · photoluminescence · tight-binding calculations

Graphene oxide (GO), atomically thin sheets of carbon with oxygen functional groups attached to both sides of the basal plane, has emerged as a "new material" that is now viewed independently from just being a precursor to graphene.[1−6] This is largely due the ability to tune its optical, electrical, electrochemical and mechanical properties through chemical modification of the oxygenated functional groups on the GO surface.[4−8] As synthesized GO is a wide band gap material with strong absorption and emission in the visible[6,9−15] and near-infrared[12] spectral regions. However, it has limited electronic conductivity due to the finite number of sp^2 clusters.[5,7,9,10,16] A key requirement of any material for its successful implementation in optoelectronic applications is its ability to absorb light and conduct the photogenerated charge carriers to the electrodes.[10] GO is potentially an ideal candidate for low-cost, large-area solution-processed optoelectronic applications because it provides

* Address correspondence to seyalcin@pnnl.gov, amohite@lanl.gov.

Received for review December 15, 2014 and accepted February 10, 2015.

Published online 10.1021/nn507150q

© XXXX American Chemical Society

an opportunity to tune both the electrical and optical properties by tuning the density of oxygenated functional groups to achieve both of these requirements. However, GO is a complex, heterogeneous and disordered system. Understanding and controlling its optoelectronic properties from mesoscale to macroscale with controlled reduction is critical for its potential induction as an active (or passive) material for thin-film optoelectronics.

A substantial amount of macroscopic measurements have aimed at understanding the evolution of the structure and density of functional groups through progressive reduction of the oxygenated functional groups using approaches such as chemical, thermal and electrochemical reductions.[7,8,10,17] Mathkar *et al.* studied the stepwise reduction of bulk GO film using hydrazine vapors and monitored the band gap using linear absorption spectroscopy.[18] Eda *et al.* elucidated the bulk optical properties of GO with progressive chemical reduction and attributed the photoluminescence to the recombination of electron−hole pairs at the localized sp^2 domains within the sp^3 (oxygenated functional groups) network.[15,19,20] Navarro *et al.* measured the electrical conductivity with progressive reduction of GO and attributed the increase in conductivity to the merging of the sp^2 domains, which creates a percolating pathway for the charge flow across the sheet.[21] Additional studies focused on investigating the electrical transport properties of GO thin-films using temperature dependent transport measurements. Their measurements demonstrates that the charge transport in GO occurs *via* a hopping mechanism.[21,22] The charge storage properties of GO and rGO have been studied using various SPM techniques.[23−26] However, it is key to probe the evolution of the intrinsic electronic properties of GO at the nanoscale when GO is getting reduced. Additionally, correlating this with the macroscopic chemical, physical and optical properties helps to identify the favorable optoelectronic state for the GO.

In this work, we have used Electrostatic Force Microscopy (EFM), optical photoluminescence (PL) imaging and theoretical tight binding calculations to understand the optoelectronic properties of GO as a function of progressive chemical reduction. We report charge injection (both positive and negative) and the subsequent visualization of migration of that injected charge on progressively reduced individual GO flakes using EFM. We demonstrate that beyond certain degrees of reduction of the GO flakes, the injected charge, independent of its polarity, can migrate to distances tens of microns depending on its reduction-state. We characterize the reduction-state of the GO flakes with its corresponding optical-state using photoluminescence imaging (see Materials and Methods section for the details of PL imaging) and electrical conductivity, and therefore elucidate the physical design principles required for engineering GO based optoelectronic applications.[1,10,20] Furthermore, our EFM measurements also reveal that the injected charge flows along the reduced GO (rGO) pathways without leaking into the adjacent GO or the less reduced region on the flake indicating the presence of an insurmountable potential barrier at the rGO/GO interface. We support our charge injection and migration experiments with theoretical modeling using quantum chemistry calculations that further demonstrate the role of barrier in regulating the charge transport. These findings provide new insights in understanding the charge propagation at the nanoscale and engineering GO/rGO based optoelectronic devices such as photo detectors, transducers based on chemical to optical detection, transparent conductors, light emitting diodes and devices.

RESULTS AND DISCUSSION

Charge Injection to As-Synthesized and Mildly Reduced GO. GO used for EFM experiments was synthesized using modified Hummers method as described previously.[9] The aqueous solution was diluted to 5×10^{-4} mg/μL and drop-casted on Si/SiO_2 substrate to obtain isolated individual GO flakes that have sizes about 30−50 μm (see Materials and Methods section for the details of sample preparation). EFM was used to visualize the charge propagation over a single GO flake. By combining atomic force microscopy (AFM, Asylum Research, MFP-3D) with conductive probes (SCM-PIT from Bruker Nano) and interleaved scanning technique, EFM measures the long-range electrostatic forces by measuring the changes in the phase relative to the oscillation frequency of the tip due to electrostatic forces acting between the tip and the GO surface.[27−29] Depending on the polarity of charge over the surface, the biased tip is attracted (or repelled) during the scan, which is represented as a bright (or dark) color code in the EFM phase image thus allowing us to infer the charge polarity/density and electric polarization properties on the surface.[22,23,30] Additionally, EFM can be used to inject charges locally and observe the migration of charges dynamically using repetitive scans on the injected area (Figure 1a).[31] This strategy has been used previously to image charge distribution in carbon nanotubes.[32,33] We have successfully used the similar approach to visualize charge propagation in electrically conductive bacterial protein filaments.[31]

For our EFM measurements, repulsive force is represented in dark color and attractive force is represented in bright color as per the phase-force curve definition in Asylum Research MFP-3D instrument.[28,29] Before charge injection experiment, an important step is to record the initial surface charge density of GO flake. In this paper, to probe the charge state, we use $V_{EFM} = \pm 5$ V. For the charge injection experiments, the tip is biased to $V_{INJ} = \pm 10$ V and intermittently touched

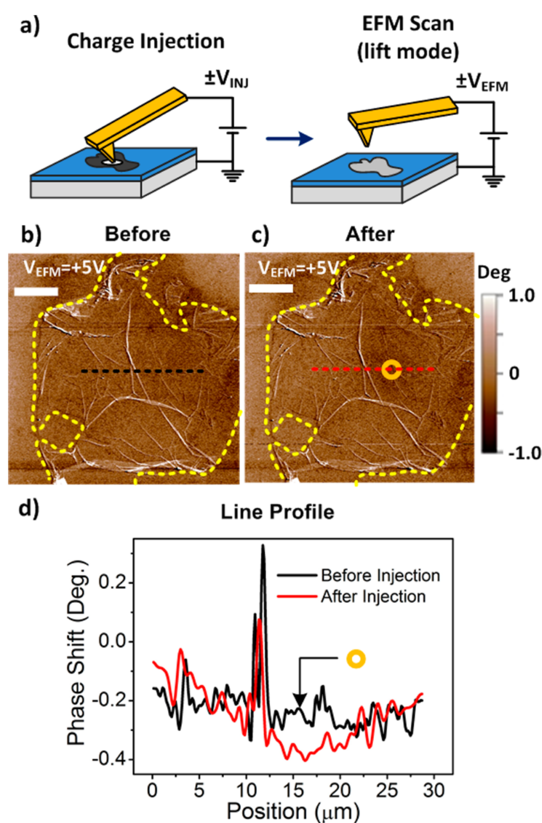

Figure 1. Charge injection experiments on pristine GO. (a) Schematic of the EFM charge injection. Charge injection ($V_{INJ} = +10$ V) is performed with the conducting tip and the charge propagation is observed using EFM lift mode with tip voltage V_{EFM}. (b) Initial charge state for $V_{EFM} = +5$ V. Yellow dashed line indicate outer edge of the GO flake. (c) EFM charge state after positive charge injection to the yellow circled point on GO flake for $V_{EFM} = +5$ V. (d) The line profile to the EFM images of before and after charge injection shows that the charge injection to the GO flake is not efficient. All scale bars in (b) and (c) are 10 μm.

to a single point on the GO flake (Figure 1a, left) (see Materials and Methods section for the details of EFM and charge injection). After the charge injection step, the tip has been lifted ~20 nm away from the surface and the probe bias of V_{EFM} is used to measure the final charge density of the GO flake (Figure 1a, right).

The EFM phase shift measures the capacitive (always attractive and proportional to V_{EFM}^2) and the Coulombic (either attractive or repulsive and proportional to V_{EFM}) interactions.[28,31,33,34] Therefore, it can be written as[28,31,33,34]

$$\Delta\Phi = C_1 V_{EFM} + C_2 V_{EFM}^2$$

where C_1 (°/V_{EFM}) and C_2 (°/V_{EFM}^2) are the fitting parameters. The injected charge enhances the Coulombic forces on the surface and can be seen by switching the V_{EFM} from positive bias to negative bias during the scan. Charge injection is confirmed when the forces change from attractive (bright color) to repulsive (dark color) in the EFM phase.

We performed charge injection and migration studies on pristine and progressively reduced GO flakes using 1% hydrazine solution for 10 min, 50 min, and 7 h (see Materials and Methods section for the hydrazine reduction procedure). Material characterization using X-ray photoelectron spectroscopy (XPS) and X-ray diffraction (XRD) confirmed that large amounts of oxygen functional groups on GO were removed after the reduction; thus, interlayer spacing between the GO sheets decreased for rGO, consistent with literatures including our previous studies (see Supporting Information Figure S2 for details).[1,3,5,15,17] The EFM on the initial charge state for pristine GO flake is given in Figure 1b. We injected positive charges at a point (yellow circle) shown in Figure 1c and the distribution of the injected charges on the GO surface were probed using positive V_{EFM}. The line profiles to the location of the charge injection before and after injection are illustrated in Figure 1d. We find that charge injection is not favorable for a pristine GO flake, consistent with its low conductivity, and is reflected as a negligible phase shift of less than 0.2°. The topography and the corresponding cross section data are shown in Supporting Information Figure S3. The EFM experiments performed on 10 min reduced GO is shown in Supporting Information Figure S4.

Figure 2 describes charge injection (positive and negative charge injection) and migration studies on a GO flake reduced for 50 min. The locations of the charge injection are represented with yellow circles (see Figure 2a,b). The dark charge cloud (repulsive forces) in Figure 2a corresponds to the injected positive charges and the bright charge cloud (attractive forces) seen in Figure 2b represents the negative charges on the same flake. With progressive scans in time (~35 min), the injected charges propagate over the rGO flake and eventually is localized at the rGO/SiO_2 boundary. This indicates that the functional groups are removed upon reduction and the conducting pathways are created for the charges to flow. The phase shift after positive/negative charge injection compared to initial charge state is illustrated in Figure 2c. From the line profile, we observe that charge propagation becomes favorable when pristine GO is converted to rGO. We attribute this facile charge transport to the formation of a percolation path of sp^2 conducting pathways with reduction. We also observe that the propensity to accept negative charges is higher in comparison to that of positive charges. We attribute this to the removal of negatively charged oxygenated surface functionalities due to hydrazine exposure, which causes the GO flake to be p-doped.[23] Furthermore, we continuously monitored the EFM phase images for the same flake after the charge injection and observed that ~85 min are required for the charges to equilibrate over the rGO surface (see Supporting Information Figure S5c,d). Additionally

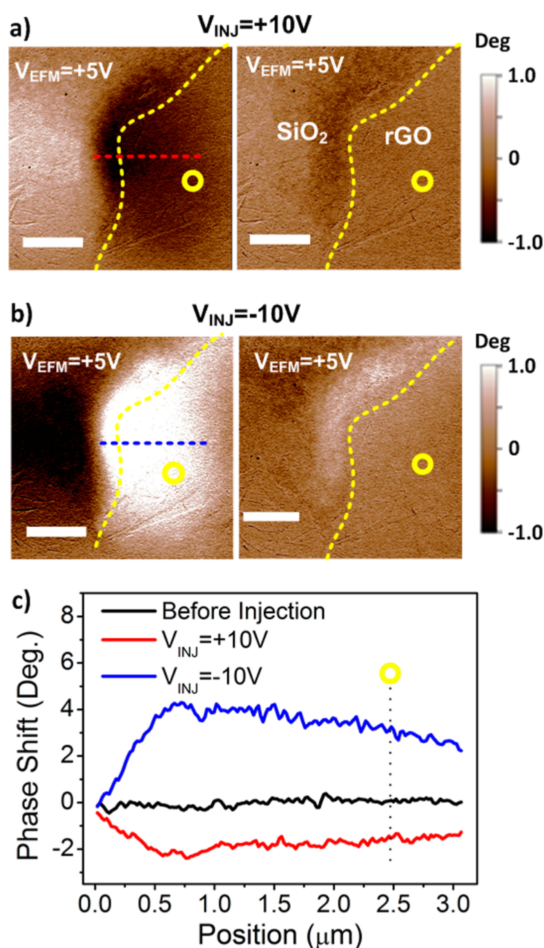

Figure 2. Charge injection experiments were performed on GO flake reduced for 50 min. Yellow dashed lines indicate the edge of the GO flake. (a) Positive charge (V_{INJ} = +10 V) is injected to the yellow circled spot on the single rGO flake. The charge state after the injection is probed with V_{EFM} = +5 V. The image shows the injected positive charges (black cloud in the EFM data) and the time evolution image acquired after 35 min (the EFM image on the right). (b) Negative charge (V_{INJ} = −10 V) injection represented with white cloud in the EFM data. The evolution of charges is probed by recording the EFM signal until the charge decays completely (see Supporting Information Figure S5d,e), (c) The cross section to the EFM phase shift data clearly shows the injected negative (blue line) and positive charges (red line) compared to the initial charge state (black line). The scale bars are 2 μm.

EFM experiments suggest that we can inject ~3 times more charges to 50 min reduced GO in comparison to the pristine GO sheet (see the EFM phase shift in Figures 1d and 2c), thus enabling direct measurement of the relative propensity of GO to accept a certain polarity of charge.

Charge Injection to Extensively Reduced GO and Proposed Charge Propagation Model. As a final step for EFM experiments on the GO flakes with different reduction times, we performed charge injection on GO flake reduced for 7 h (Figure 3). Figure 3a represents the initial charge state (See Supporting Information, Figure S6a for the AFM topography of the flake and Figure S6b for the cross section of the height profile.) Figure 3b illustrates the location of the charge injection (yellow circle) that we selected as a first point to inject charge for the 7 h reduced GO flake. The subsequent EFM scans are taken with both positive (Supporting Information Figure S6d) and negative (Supporting Information Figure S6e) tip bias. We did not observe any noticeable change in the charged state for the 7 h rGO in comparison with the initial state for both positive and negative charge injection to the basal plane (Supporting Information Figure S6c−e). We attribute this to the highly conductive nature of rGO, where the injected charge can rapidly (faster than the EFM scan duration) decay and equilibrate bringing the flake to its original state. However, clues to understanding the charge propagation on a completely reduced GO flake can be obtained by injecting charge onto the wrinkled network on the rGO flake. We injected positive charges on one end of a wrinkle represented by a red circle in Figure 3b. The line profiles to the EFM phase images before and after charge injection are illustrated in Figure 3c. After positive charge injection, when the bias on the tip is switched from positive (V_{EFM} = +5 V) to negative (V_{EFM} = −5 V), the EFM force changes from repulsive to attractive only on the wrinkle (Figure 3c), while the basal plane remains unchanged. This is observed as a change in the color contrast from gray (V_{EFM} = +5 V) to bright (V_{EFM} = −5 V) on the wrinkle network. From the change in phase, we conclude that the charges can efficiently propagate over a distance of >50 μm. We also performed these experiments with a negative charge injection (V_{INJ} = −10 V) to the same flake after the flake returned to its original charge state. For negative charge injection to the wrinkle on the flake, we observed a similar behavior, where the force changes from attractive to repulsive when the bias is switched from V_{EFM} = +5 V to V_{EFM} = −5 V (Supporting Information Figure S6f,g). Notably, for the same charge injection bias, independent of the polarity, the charge propagation is confined to the wrinkled network and does not leak over to the basal plane.

We know that the charge propagation mainly occur over sp^2 conducting pathways. This suggests that the top surface of the wrinkled network and the basal plane is predominantly reduced after hydrazine exposure and forms a continuous sp^2 pathway for the injected charge to flow along the contours defined by the wrinkle. However, the injected charge from the wrinkle or the basal plane does not leak over to the other side. On the basis of these observations, we hypothesize that there must exist a large potential barrier between the top of the wrinkle and the basal plane due to the presence of oxygenated functional groups trapped between the wrinkle and the rGO plane. The schematic for our hypothesis is illustrated in Figure 3d,e. Yellow regions in Figure 3d represent the part of the GO sheet where the reduction is incomplete because the hydrazine is unable to diffuse

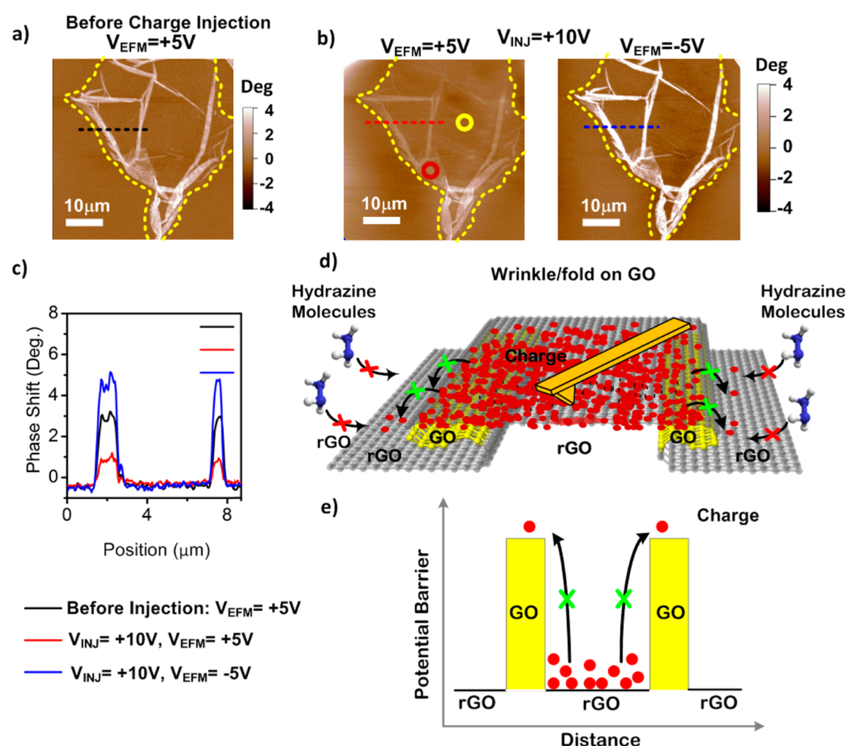

Figure 3. Charge injection experiments were performed on 7 h reduced (rGO) flake. (a) Initial charge state is probed with $V_{EFM} = +5$ V. As a first step, positive charge ($V_{INJ} = +10$ V) is injected to the yellow circled spot on the basal plane of rGO. As a second step, (b) positive ($V_{INJ} = +10$ V) and negative charges ($V_{INJ} = -10$ V) are injected to the red circled spot on the wrinkle of rGO. See Supporting Information Figure S6f,g for the EFM negative charge injection to the wrinkle. (c) The cross section to the EFM phase shift data (black, red and blue dotted lines are shown on parts (a) and (b)). Switching the polarity of the probe changes the EFM phase shift which is the indication of the propagation of the injected charge only over the wrinkle. (d) The schematic of a wrinkle on the GO flake. The injected charges are shown with red solid circles. Yellow region below the wrinkle represent the unreduced GO after hydrazine exposure. (e) The schematic of the potential barrier that shows the prohibition of charge propagation. All the scale bars on the EFM images are 10 μm.

to the trapped region underneath the wrinkle. This is assumed to create a potential barrier for the injected charges to migrate from the wrinkle to the basal plane of GO or *vice versa* (Figure 3e), thus limiting the charge transport along the wrinkled contours on the rGO.

Correlation with Photoluminescence Results. To corroborate the presence of trapped oxygenated functional groups under the wrinkles and folds, we correlated our EFM experiments with the fluorescence imaging of GO, progressively reduced with the same reduction times used for the EFM measurements (see Supporting Information Figure S1 for the PL imaging details and Supporting Information Figure S7 for the images). One of the accepted origins of PL in GO is from the states in the close proximity to the functional groups,[6,9] and thus, the spatial distribution of the PL intensity on the flake can be used to quantitatively compare the density of functional groups on the flake. The GO sheet was continuously imaged as it was reduced by the hydrazine solution, over the course of the ~7 h and shown in Supporting Information Figure S7 (corresponding reduction times are included on each of GO images). The wrinkles on the GO flake appear as bright red-lines on the PL image, representing a higher density of oxygenated functional groups trapped under the folds. Even at high degrees of reduction time, the wrinkles on the GO sheets remain relatively bright even as the surrounding areas have reduced their intensity, indicating that the wrinkles are not reduced efficiently thus confirming our hypothesis that the charge flow from the top of the wrinkle/fold to the basal plane is efficiently hindered by the presence of unreduced functional groups trapped under the fold, even after long reduction times.

EFM charge injection experiments on GO as a function of different reduction times allows us to extract an effective charge migration distance ($L_{distance}$). For the same reduction times, we measure the electrical conductivity. This gives us a correlation between $L_{distance}$ and the corresponding electrical conductivity. Combining the results obtained using EFM, PL imaging, and electrical transport measurements, we obtain a relationship between the three physical figures of merit that describe the GO (Figure 4).

The intersection region of the curves (depicted by a yellow oval) represents the regime where the GO is optically active (absorbs light) and also electrically conductive. Deviating away from the yellow oval results in a state that is nonideal for optoelectronic applications, and thus, represents a simple approach

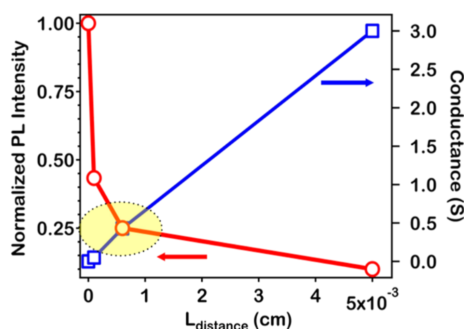

Figure 4. Normalized PL intensity and measured electrical conductivity plotted as a function of charge migration distance acquired using EFM experiments. The intersection of the three physical quantities is represented by the yellow oval and corresponds to a state of GO that is optically active and electrically conducting.

that could be applied for the fabrication of GO-based, low-cost optoelectronic applications.

GO/rGO/GO Ribbon Patterns and Tight-Binding Calculations. Motivated by our EFM and PL observations, we experimentally mimic an rGO/GO interface (similar to the wrinkle depicted in Figure 3d,e to gain a deeper understanding of the rGO/GO boundary, by intentionally patterning a GO/rGO/GO ribbon using e-beam lithography and hydrazine reduction (see Materials and Methods section for the details). We performed charge injection experiments (similar to those described in Figures 1−3) on the rGO region of the ribbon by gently touching with the conducting tip and injecting negative charge (V_{INJ} = −10 V) to the point shown as a yellow circle in Figure 5a. The EFM signal was probed with positive bias on the tip. After the negative charge injection (the bright charge cloud in Figure 5a), electrons propagate predominantly along the rGO and do not leak over to the GO region suggesting that indeed there is a large potential barrier at the rGO/GO interface.

To gain additional insights into the mechanism of charge transport, we performed tight-binding calculations of graphene[35,36] and graphene oxide to model the EFM experiments on intentionally patterned GO/rGO/GO ribbons. Supporting Information Figure S8 shows the dependence of inverse participation ratio (IPR) for electronic states of the tight-binding model on $f_{sp}{}^3$ (the fraction of sp^3-hybridized carbon atoms). IPR is defined as an intuitive measure of the degree of localization of electronic states, and thus, if an electronic states is delocalized over N carbon atoms, then the corresponding IPR is ∼1/N.

Since the degree of delocalization of electronic states defines the electronic conductivity, 1/IPR can be thought of as a measure of rGO conductivity in our tight-binding calculations. The conductivity is then seen to increase rapidly when GO is reduced, *i.e.*, when f_{sp^3} decreases (see Supporting Information for details). Specifically, a thin vertical stripe in the middle of the flake has a relatively low concentration of sp^3 carbons

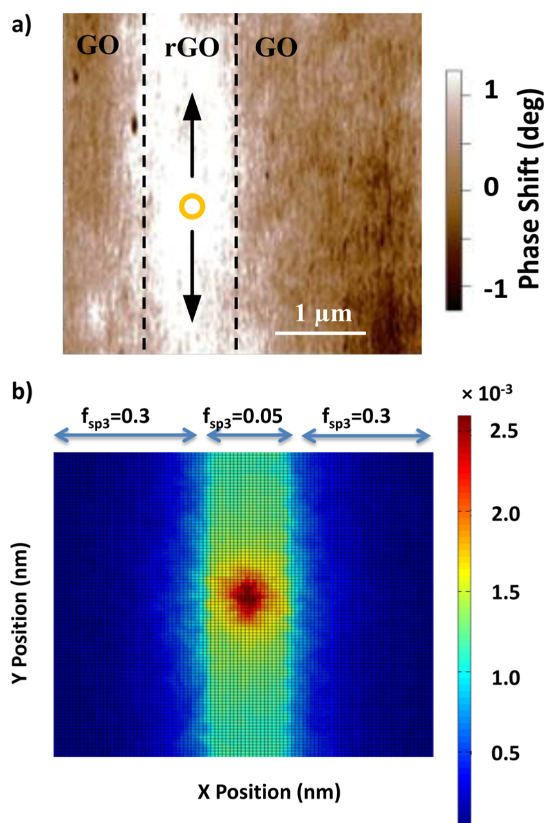

Figure 5. EFM charge injection and detection experiments on patterned rGO ribbon and corresponding tight binding calculations. (a) EFM phase shift image of patterned GO flake after negative charge injection (V_{INJ} = −10 V) and V_{EFM} = +5 V. Charge injection point is given with yellow circle and the charge (white cloud) propagates only through the rGO. (b) Density plot of the charge density obtained by tight-binding simulations of charge injection at the center of the graphene flake with a nonuniform distribution of sp^3-hybridized carbon atoms.

(f_{sp^3} = 0.05), whereas the rest of the flake has a high concentration of functional groups (f_{sp^3} = 0.3). The result of the charge injection at the center of the charge-conducting stripe is shown in Figure 5b as a density plot. The charges preferentially propagate only along the rGO stripe, thus illustrating and supporting our experimental EFM observations of potential barrier for the charge flow from rGO to GO plane seen in Figure 5a and schematically drawn in Figure 3e.

CONCLUSIONS

We directly correlate the electrical state of progressively reduced GO with its corresponding optical state using a suite of techniques: EFM, electrical conductivity and photoluminescence imaging. These measurements elucidate the optimal electrical and optical properties required for achieving low-cost, GO based thin-film optoelectronic applications. Furthermore, these results have important implications in understanding the mechanism of charge propagation in GO to facilitate the fabrication of high-performance GO devices. From a broader perspective, the experimental approach

using EFM to determine the effective charge propagation length might find widespread applications in other layered materials such as transition metal dichalcogenides.

MATERIALS AND METHODS

Photoluminescence Imaging of Individual Graphene Oxide (GO) Sheets. The single-molecule imaging and spectroscopy setup consists of an inverted confocal microscope with a 100×, NA 1.49 objective. A 405 nm, 70 ps pulsed laser is used to excite the sample with an approximate spot diameter of ≈300 nm. The excitation beam is reflected by a scanning mirror before entering the objective. The scanning mirror can be used to steer the focused beam in the *XY* focal plane of the objective, in an approximate maximum area of 90 × 90 μm^2. The collected fluorescence is separated from the excitation by using a dichroic mirror having a 450−700 nm transmission range and detected using an avalanche photodiode (APD). When we rasterize the beam over the sample and collect the PL intensity at each point, a fluorescence image of the sample is built. A cuvette with a hole cut into its bottom was stuck onto the coverslip (Supporting Information Figure S1). A very dilute dispersion of GO in water is carefully cast onto a quartz coverslip.

Sample Preparation and Hydrazine Reduction Procedure. *Sample Cleaning.* Prepatterned silicon chips capped with 300 nm of oxide layer have been used as a substrate to drop cast the GO. Before the dropcast procedure, the chips have been sonicated for 10 min with acetone and then rinsed with IPA.

Hydrazine Reduction. For the hydrazine reduction procedure, we have used hydrazine hydrate with 25% in H_2O (Sigma-Aldrich, Product No: 53847). GO drop-casted samples were dipped to 1% hydrazine solutions for 10 min, 50 min, and 7 h. The reaction has been stopped by dipping the reduced GO samples in deionized (DI) water.

Electrostatic Force Microscopy (EFM) Technical Details. *Probe Properties.* Conductive EFM tips (oscillation frequency $f_0 \approx 60$ kHz and spring constant $k \approx 1.5$, nominally 2.8 N/m) were coated with 20 nm Pt/Ir to provide an electrical connection from the cantilever to the tip apex.[28]

EFM Technique. The technique is based on two pass scans: in the first pass of the scan, the tip stays near to the surface and measures the strong van der Waals forces to get the topography of the sample through intermittent contact imaging (Supporting Information Figure S3a). In the second pass of the scan, known as an interleaved scan, the tip is lifted away from the surface and a dc bias is applied to the probe (Supporting Information Figure S3b). The lift height calibration for the interleave scan is an important step to avoid any topography contribution in the EFM signal enabling accurate measurement of long-range electrostatic forces.[28,31]

Lift Height Calibration. The lift height calibration for the interleave scan is an important step to avoid any topography contribution in the EFM signal.[31] For this calibration procedure, the oscillation amplitude of the tip is significantly reduced compared to the first pass scan. Then the tip is kept unbiased, gradually reduced to the surface of the sample and the EFM phase shift is recorded simultaneously. Once the tip starts showing topography signal on the EFM phase shift, the tip is lifted 20 nm away from the surface and the EFM phase shift is watched until it goes to zero. Due to this careful calibration step, we know that we only measure long-range electrostatic forces.[31]

Charge Injection with EFM. For the charge injection experiments, we used typical injection voltages of $V_{INJ} = \pm 10$ V.[31,37] The biased tip is intermittently touched to a single point on the GO flake (Figure1a). This is called sweep mode and the tip touches to single point on GO for 1 s, then retracts for 5 s, and this procedure repeats for total 1 min. During the charge injection, the phase-force curve of the tip is recorded which allows us to see the applied force to the surface that lies in the range of nN. This is an important step to secure any possible damage to tip or to the GO flake during the injection experiment.

Lithography Details for the GO/rGO/GO Ribbon. After locating suitable GO flakes through optical microscopy, we coated the samples with PMMA at 3000 rpm for 60 s and baked them at 180 °C for 90 s. We exposed areas on the GO flake using e-beam lithography. The rGO strip had 1 μm width and 4 μm lengths (Figure 5a). The patterned rGO line has been chemically reduced using 5% hydrazine for 10 min while GO part has been protected from hydrazine due to PMMA, allowing the reduction chemistry happening only in the center (rGO part). Due to this controlled reduction, we only have conducting percolating pathways in the plane of rGO, whereas the GO preserves sp^3 hybridization. Then the PMMA on the sample were removed using acetone followed by an IPA rinse.

Tight Binding Calculations. Details are presented in Supporting Information.

Conflict of Interest: The authors declare no competing financial interest.

Acknowledgment. This work was supported by the LANL LDRD program (XW5A and XW5X). The work was conducted, in part, at the Center for Integrated Nanotechnologies (CINT), a U.S. Department of Energy, and Office of Basic Energy Sciences (OBES) user facility. The authors thank Gabriel A. Montano for the use of Asylum Research MFP-3D, Nikhil S. Malvankar for the helpful discussions on electrical measurements and EFM imaging, and Jinkyoung Yoo for the support.

Supporting Information Available: Experimental setup information on scanning confocal microscopy system used for photoluminescence imaging of individual graphene oxide (GO) sheets (Figure S1). Material characterization of rGO (Figure S2). The schematic of the EFM experiment and the AFM height profile for pristine GO (Figure S3). EFM charge injection experiments on 10 min reduced (1% hydrazine) GO sheet (Figure S4). EFM charge injection experiments on 50 min reduced (1% hydrazine) GO sheet (Figure S5). AFM images on 7 h reduced (1% hydrazine) GO sheet (Figure S6). PL images of *in situ* progressively rGO sheet over the course of ~7 h of exposure to 1% hydrazine solution (Figure S7). Inverse participation ratio for electronic states in rGO at different concentration of sp^3-hybridized carbon atoms (Figure S8). Charge density of GO and rGO using tight-binding calculations (Figure S9). This material is available free of charge *via* the Internet at http://pubs.acs.org.

REFERENCES AND NOTES

1. Eda, G.; Fanchini, G.; Chhowalla, M. Large-Area Ultrathin Films of Reduced Graphene Oxide as a Transparent and Flexible Electronic Material. *Nat. Nanotechnol.* **2008**, *3*, 270–274.
2. Stankovich, S.; Dikin, D. A.; Dommett, G. H.; Kohlhaas, K. M.; Zimney, E. J.; Stach, E. A.; Piner, R. D.; Nguyen, S. T.; Ruoff, R. S. Graphene-Based Composite Materials. *Nature* **2006**, *442*, 282–286.
3. Stankovich, S.; Dikin, D. A.; Piner, R. D.; Kohlhaas, K. A.; Kleinhammes, A.; Jia, Y.; Wu, Y.; Nguyen, S. T.; Ruoff, R. S. Synthesis of Graphene-Based Nanosheets *via* Chemical Reduction of Exfoliated Graphite Oxide. *Carbon* **2007**, *45*, 1558–1565.
4. Stankovich, S.; Piner, R. D.; Chen, X.; Wu, N.; Nguyen, S. T.; Ruoff, R. S. Stable Aqueous Dispersions of Graphitic Nanoplatelets *via* the Reduction of Exfoliated Graphite Oxide in the Presence of Poly (Sodium 4-Styrenesulfonate). *J. Mater. Chem.* **2006**, *16*, 155–158.
5. Gao, W.; Alemany, L. B.; Ci, L.; Ajayan, P. M. New Insights into the Structure and Reduction of Graphite Oxide. *Nat. Chem.* **2009**, *1*, 403–408.

6. Galande, C.; Gao, W.; Mathkar, A.; Dattelbaum, A. M.; Narayanan, T. N.; Mohite, A. D.; Ajayan, P. M. Science and Engineering of Graphene Oxide. *Part. Part. Syst. Charact.* **2014**, *31*, 619–638.
7. Dreyer, D. R.; Park, S.; Bielawski, C. W.; Ruoff, R. S. The Chemistry of Graphene Oxide. *Chem. Soc. Rev.* **2010**, *39*, 228–240.
8. Mattevi, C.; Eda, G.; Agnoli, S.; Miller, S.; Mkhoyan, K. A.; Celik, O.; Mastrogiovanni, D.; Granozzi, G.; Garfunkel, E.; Chhowalla, M. Evolution of Electrical, Chemical, and Structural Properties of Transparent and Conducting Chemically Derived Graphene Thin Films. *Adv. Funct. Mater.* **2009**, *19*, 2577–2583.
9. Galande, C.; Mohite, A. D.; Naumov, A. V.; Gao, W.; Ci, L.; Ajayan, A.; Gao, H.; Srivastava, A.; Weisman, R. B.; Ajayan, P. M. Quasi-Molecular Fluorescence from Graphene Oxide. *Sci. Rep.* **2011**, 1.
10. Loh, K. P.; Bao, Q.; Eda, G.; Chhowalla, M. Graphene Oxide as a Chemically Tunable Platform for Optical Applications. *Nat. Chem.* **2010**, *2*, 1015–1024.
11. Sun, X.; Liu, Z.; Welsher, K.; Robinson, J. T.; Goodwin, A.; Zaric, S.; Dai, H. Nano-Graphene Oxide for Cellular Imaging and Drug Delivery. *Nano Res.* **2008**, *1*, 203–212.
12. Luo, Z.; Vora, P. M.; Mele, E. J.; Johnson, A. C.; Kikkawa, J. M. Photoluminescence and Band Gap Modulation in Graphene Oxide. *Appl. Phys. Lett.* **2009**, *94*, 111909.
13. Williams, G.; Kamat, P. V. Graphene– Semiconductor Nanocomposites: Excited-State Interactions between ZnO Nanoparticles and Graphene Oxide. *Langmuir* **2009**, *25*, 13869–13873.
14. Sokolov, D. A.; Morozov, Y. V.; McDonald, M. P.; Vietmeyer, F.; Hodak, J. H.; Kuno, M. Direct Observation of Single Layer Graphene Oxide Reduction through Spatially-Resolved, Single Sheet Absorption/Emission Microscopy. *Nano Lett.* **2014**, *14*, 3172–3179.
15. Eda, G.; Lin, Y. Y.; Mattevi, C.; Yamaguchi, H.; Chen, H. A.; Chen, I.; Chen, C. W.; Chhowalla, M. Blue Photoluminescence from Chemically Derived Graphene Oxide. *Adv. Mater.* **2010**, *22*, 505–509.
16. Bagri, A.; Mattevi, C.; Acik, M.; Chabal, Y. J.; Chhowalla, M.; Shenoy, V. B. Structural Evolution during the Reduction of Chemically Derived Graphene Oxide. *Nat. Chem.* **2010**, *2*, 581–587.
17. Eda, G.; Mattevi, C.; Yamaguchi, H.; Kim, H.; Chhowalla, M. Insulator to Semimetal Transition in Graphene Oxide. *J. Phys. Chem. C* **2009**, *113*, 15768–15771.
18. Mathkar, A.; Tozier, D.; Cox, P.; Ong, P.; Galande, C.; Balakrishnan, K.; Leela Mohana Reddy, A.; Ajayan, P. M. Controlled, Stepwise Reduction and Band Gap Manipulation of Graphene Oxide. *J. Phys. Chem. Lett.* **2012**, *3*, 986–991.
19. Eda, G.; Ball, J.; Mattevi, C.; Acik, M.; Artiglia, L.; Granozzi, G.; Chabal, Y.; Anthopoulos, T. D.; Chhowalla, M. Partially Oxidized Graphene as a Precursor to Graphene. *J. Mater. Chem.* **2011**, *21*, 11217–11223.
20. Eda, G.; Chhowalla, M. Chemically Derived Graphene Oxide: Towards Large-Area Thin-Film Electronics and Optoelectronics. *Adv. Mater.* **2010**, *22*, 2392–2415.
21. Gómez-Navarro, C.; Weitz, R. T.; Bittner, A. M.; Scolari, M.; Mews, A.; Burghard, M.; Kern, K. Electronic Transport Properties of Individual Chemically Reduced Graphene Oxide Sheets. *Nano Lett.* **2007**, *7*, 3499–3503.
22. Venugopal, G.; Krishnamoorthy, K.; Mohan, R.; Kim, S.-J. An Investigation of the Electrical Transport Properties of Graphene-Oxide Thin Films. *Mater. Chem. Phys.* **2012**, *132*, 29–33.
23. Kulkarni, D. D.; Kim, S.; Chyasnavichyus, M.; Hu, K.; Fedorov, A. G.; Tsukruk, V. V. Chemical Reduction of Individual Graphene Oxide Sheets as Revealed by Electrostatic Force Microscopy. *J. Am. Chem. Soc.* **2014**, *136*, 6546–6549.
24. Wei, Z.; Wang, D.; Kim, S.; Kim, S.-Y.; Hu, Y.; Yakes, M. K.; Laracuente, A. R.; Dai, Z.; Marder, S. R.; Berger, C.; et al. Nanoscale Tunable Reduction of Graphene Oxide for Graphene Electronics. *Science* **2010**, *328*, 1373–1376.
25. Wang, Y.; Shen, Y.; Zhang, X.; Zhang, Y.; Hu, J. Humidity Induced Charge Migration on Single Layer Graphene Oxide Sheets. *Appl. Phys. Lett.* **2014**, *105*, 233107.
26. Shen, Y.; Guo, S.; Hu, J.; Zhang, Y. Charging of Nanostructured and Partially Reduced Graphene Oxide Sheets. *Appl. Phys. Lett.* **2012**, *101*, 183109.
27. Bonnell, D. A. *Scanning Probe Microscopy and Spectroscopy: Theory, Techniques, and Applications*; Wiley-VCH: New York, 2001.
28. Yalcin, S. E.; Labastide, J. A.; Sowle, D. L.; Barnes, M. D. Spectral Properties of Multiply Charged Semiconductor Quantum Dots. *Nano Lett.* **2011**, *11*, 4425–4430.
29. Yalcin, S. E.; Yang, B.; Labastide, J. A.; Barnes, M. D. Electrostatic Force Microscopy and Spectral Studies of Electron Attachment to Single Quantum Dots on Indium Tin Oxide Substrates. *J. Phys. Chem. C* **2012**, *116*, 15847–15853.
30. Esteban-Ferrer, D.; Edwards, M. A.; Fumagalli, L.; Juárez, A.; Gomila, G. Electric Polarization Properties of Single Bacteria Measured with Electrostatic Force Microscopy. *ACS Nano* **2014**, *8*, 9843–9849.
31. Malvankar, N. S.; Yalcin, S. E.; Tuominen, M. T.; Lovley, D. R. Visualization of Charge Propagation along Individual Pili Proteins Using Ambient Electrostatic Force Microscopy. *Nat. Nanotechnol.* **2014**, *9*, 1012–1017.
32. Mélin, T.; Diesinger, H.; Deresmes, D.; Stiévenard, D. Probing Nanoscale Dipole-Dipole Interactions by Electric Force Microscopy. *Phys. Rev. Lett.* **2004**, *92*, 166101.
33. Mélin, T.; Zdrojek, M.; Brunel, D. Electrostatic Force Microscopy and Kelvin Force Microscopy as a Probe of the Electrostatic and Electronic Properties of Carbon Nanotubes. In *Scanning Probe Microscopy in Nanoscience and Nanotechnology*; Springer: Heidelberg, 2010; 89–128.
34. Heim, T.; Lmimouni, K.; Vuillaume, D. Ambipolar Charge Injection and Transport in a Single Pentacene Monolayer Island. *Nano Lett.* **2004**, *4*, 2145–2150.
35. Wallace, P. R. The Band Theory of Graphite. *Phys. Rev.* **1947**, *71*, 622.
36. Neto, A. C.; Guinea, F.; Peres, N.; Novoselov, K. S.; Geim, A. K. The Electronic Properties of Graphene. *Rev. Mod. Phys.* **2009**, *81*, 109.
37. Bhushan, B. *Scanning Probe Microscopy in Nanoscience and Nanotechnology*. Springer: Heidelberg, 2010; Vol. 1.